# Local Density of States for Nanoplasmonics

Tigran V. Shahbazyan

Phys. Rev. Lett. **117**, 207401 — Published 8 November 2016

DOI: 10.1103/PhysRevLett.117.207401

# Local Density of States for Nanoplasmonics

Tigran V. Shahbazyan
*Department of Physics, Jackson State University, Jackson, MS 39217 USA*
(Dated: Monday 10th October, 2016, 16:40)

We obtain local density of states (LDOS) for any nanoplasmonic system in the frequency range dominated by a localized plasmon. By including the Ohmic losses in a consistent way, we show that the plasmon LDOS is proportional to the local field intensity normalized by the absorbed power. We obtain explicit formulae for energy transfer (ET) between quantum emitters and plasmons as well as between donors and acceptors situated near a plasmonic structure. In the latter case, we find that the plasmon-assisted ET rate is proportional to the LDOS product at the donor and acceptor positions, obtain, in a general form, the plasmon ET enhancement factor, and establish the transition onset between Förster-dominated and plasmon-dominated ET regimes.

Rapid advances in nanoplasmonics of the past decade opened up possibilities for energy concentration and transfer at the lengthscales well below the diffraction limit [1]. Optical interactions between dye molecules or semiconductor quantum dots, hereafter referred to as quantum emitters (QE), and localized plasmons in metal-dielectric composite nanostructures underpin major phenomena in plasmon-enhanced spectroscopy, including surface-enhanced Raman scattering [2], plasmon-assisted fluorescence [3–5] and energy transfer [6–8], strong QE-plasmon coupling [9–11], and plasmonic laser (spaser) [12–14]. The interactions of a QE, located at $\boldsymbol{r}$, with electromagnetic modes are characterized by the local density of states (LDOS), $\rho(\omega,\boldsymbol{r}) = (2\omega/\pi c^2)\mathrm{Im}[\mathrm{Tr}\bar{\mathbf{G}}(\omega;\boldsymbol{r},\boldsymbol{r})]$, where $\bar{\mathbf{G}}(\omega;\boldsymbol{r},\boldsymbol{r}')$ is the electromagnetic Green dyadic and $c$ and $\omega$ are speed and frequencyof light, which represents the number of modes in unit volume and frequency interval [15]. In particular, the LDOS quantifies the Purcell enhancement of spontaneous emission by a QE in a photonic environment [16], e.g., near metal surfaces [17–20], metamaterials [21, 22], or plasmonic nanostructures [23–26]. A closely related quantity, the cross density of states (CDOS), $\rho(\omega;\boldsymbol{r},\boldsymbol{r}') = (2\omega/\pi c^2)\mathrm{Im}[\mathrm{Tr}\bar{\mathbf{G}}(\omega;\boldsymbol{r},\boldsymbol{r}')]$, describes spatial correlations, e.g., due to indirect coupling between QEs [27]. While for high-symmetry systems, such as flat surfaces or spherical particles, the electromagnetic LDOS is known, its calculation for general-shape systems presents a rather challanging task. A photon emission by a QE involves all system eigenmodes that define the continuum of final states [28, 29], so that in open systems, the calculations of LDOS and CDOS rely on carefully defined quasinormal modes [30, 31].

At the same time, nanoplasmonic systems support a host of phenomena that are underpinned by *nonradiative* plasmon-assisted transitions. For example, the energy transfer (ET) rate between QEs and plasmons, whose frequencies are tuned to resonance, is among the key characteristics in plasmonics applications such as biosensing [32, 33]. The magnitude and range of the Förster's ET between a donor and an acceptor near a plasmonic structure is strongly enhanced by plasmon-mediated ET channel [35–38], while the role of LDOS in the enhancement mechanism is a subject of ongoing debate [39–47]. Other examples of coherent plasmon-assisted processes include strong QE-plasmon coupling [48, 49] and spaser [50]. Such phenomena hinge on QEs coupling to resonant plasmon modes characterized by the *plasmon* LDOS (or CDOS), which, in general, can be obtained from the electromagnetic LDOS in the near-field limit. On the other hand, in the frequency region dominated by a localized plasmon mode, one expects the plasmon LDOS to be determined *directly* by the mode local field. At the same time, for system size below the diffraction limit, the plasmon decay is mainly due to the Ohmic losses in metal, while radiation plays a relatively minor role [1]. Therefore, an accurate theory for plasmon LDOS must rely on the consistent treatment of Ohmic losses.

Here, we derive the plasmon LDOS (and CDOS) in terms of plasmon local fields for any nanoplasmonic system described by a local dielectric function $\varepsilon(\omega,\mathbf{r}) = \varepsilon'(\omega,\mathbf{r}) + i\varepsilon''(\omega,\mathbf{r})$. Namely, for $\omega$ near the plasmon frequency $\omega_n$, the LDOS has a universal form

$$\rho(\omega_n,\boldsymbol{r}) = \frac{2}{\pi\omega_n}\frac{|\mathbf{E}_n(\boldsymbol{r})|^2}{\int dV\varepsilon''|\mathbf{E}_n|^2}, \tag{1}$$

where $\mathbf{E}_n(\boldsymbol{r})$ is the local field determined by the Gauss's law $\boldsymbol{\nabla}\cdot[\varepsilon'(\omega_n,\boldsymbol{r})\mathbf{E}_n(\boldsymbol{r})] = 0$, and integration in is carried over the system volume. The plasmon LDOS is proportional to the local field intensity normalized by the absorbed power. Derivation of Eq. (1), outlined below, involves a consistent treatment of the Ohmic losses, which determine the plasmon decay rate $\gamma_n$, and implies a well-defined plasmon with quality factor $q_n = \omega_n/\gamma_n \gg 1$. With LDOS (1) and the corresponding CDOS, we obtain the QE-plasmon ET rates as well as the donor-acceptor Förster ET rate near a plasmonic structure. In the latter case, the rate is proportional to the LDOS product at the donor and acceptor positions. We derive the plasmon ET enhancement factor and establish a general condition that governs the transition between Förster-dominated and plasmon-dominated ET regimes. Finally, for an ensemble of QEs coupled to a resonant plasmon mode, we derive cooperative ET rate in terms of LDOS for individual QEs which scales with the ensemble size.

***Theory***.—We consider a metal-dielectric nanostructure supporting localized plasmon modes that is characterized by dielectric function $\varepsilon(\omega,\boldsymbol{r})=1+4\pi\sum_i\chi_i(\omega,\boldsymbol{r})$, where $\chi_i(\omega,\boldsymbol{r})=\Theta_i(\boldsymbol{r})[\varepsilon_i(\omega)-1]/4\pi$ are the local susceptibilities; $\Theta_i(\boldsymbol{r})$ is 1 in the region $V_i$ with dielectric function $\varepsilon_i$ and is 0 outside of it. We assume that only in *metallic* regions are the dielectric functions $\varepsilon_m(\omega)$ dispersive and complex and that the retardation effects are unimportant. The susceptibilities $\chi_i$ define the polarization vector $\mathbf{P}(\boldsymbol{r})=\sum_i\chi_i(\omega,\mathbf{r})\mathbf{E}(\boldsymbol{r})$, where $\mathbf{E}=-\boldsymbol{\nabla}\Phi$ is the local field and $\Phi(\boldsymbol{r})$ is the potential.

Our goal is to derive the plasmon Green function and, hence, the LDOS by including, in a consistent way, the Ohmic losses that give rise to the plasmon decay rate $\gamma_n$. We assume that plasmon modes are well defined, i.e., $q_n=\omega_n/\gamma_n\gg1$, and adopt perturbative approach with respect to $1/q_n$. We start with self-consistent microscopic equation for the potential $\Phi(\boldsymbol{r})$ [51],

$$\Phi(\boldsymbol{r})=\varphi(\boldsymbol{r})+\int dV_1dV_2u(\boldsymbol{r}-\boldsymbol{r}_1)P(\boldsymbol{r}_1,\boldsymbol{r}_2)\Phi(\boldsymbol{r}_2),\quad(2)$$

where $\hat{P}=\hat{P}'+i\hat{P}''$ is the electron polarization operator, $u(r)=1/r$ is the Coulomb potential (we set the electron charge to unity), and $\varphi(\boldsymbol{r})$ is an external potential. The system eigenmodes are described by the homogeneous part of Eq. (2), which we write as $(\Delta+4\pi\hat{P})\Phi=0$, where we used that $\Delta u(\boldsymbol{r}-\boldsymbol{r}')=-4\pi\delta(\boldsymbol{r}-\boldsymbol{r}')$. The operator $\hat{P}$ is related to the polarization vector $\mathbf{P}$ via the induced charge density: $\rho(\boldsymbol{r})=\int d\boldsymbol{r}'P(\boldsymbol{r},\boldsymbol{r}')\Phi(\boldsymbol{r}')=-\boldsymbol{\nabla}\cdot\mathbf{P}(\boldsymbol{r})$. In the *local* case, we have $\boldsymbol{\nabla}\cdot\mathbf{P}(\boldsymbol{r})=\sum_i\boldsymbol{\nabla}\cdot[\chi_i(\boldsymbol{r})\mathbf{E}(\boldsymbol{r})]$, and the polarization operator takes the form

$$P(\omega;\boldsymbol{r},\boldsymbol{r}')=\sum_i\boldsymbol{\nabla}\cdot\left[\chi_i(\omega,\boldsymbol{r})\boldsymbol{\nabla}\delta(\boldsymbol{r}-\boldsymbol{r}')\right].\quad(3)$$

We now introduce eigenfunctions $\Phi_n(\boldsymbol{r})$ and eigenvalues $\lambda_n(\omega)$ of the *real* part of polarization operator as

$$4\pi\hat{P}'\Phi_n\equiv4\pi\sum_i\boldsymbol{\nabla}\cdot(\chi_i'\boldsymbol{\nabla}\Phi_n)=\lambda_n\Delta\Phi_n.\quad(4)$$

Since $\Phi_n(\boldsymbol{r})$ are harmonic in each region and continuous at the interfaces, they must be regular inside the nanostructure and decay sufficiently fast outside of it. Note that this approach resembles the eigenvalue problem in binary systems [1, 52], but with the key difference that here the eigenvalues depend on the system dielectric function, allowing us to include the losses in a consistent way. From Eq. (4), the modes orthogonality follows: $\int dV\mathbf{E}_m\cdot\mathbf{E}_n=\delta_{mn}\int dV\mathbf{E}_n^2$. Note that the eigenfunctions of $\hat{P}'$ can always be chosen real. From Eq. (4), the eigenvalues are given by $\lambda_n=4\pi\langle n|\hat{P}'|n\rangle/\langle n|\hat{\Delta}|n\rangle$. To find eigenfrequencies $\omega_n$, we write this expression as

$$1+\lambda_n(\omega)=\sum_i\varepsilon_i'\frac{\int dV_i\mathbf{E}_n^2}{\int dV\mathbf{E}_n^2}=\frac{\int dV\varepsilon'(\omega,\boldsymbol{r})\mathbf{E}_n^2}{\int dV\mathbf{E}_n^2}.\quad(5)$$

For $\omega=\omega_n$, the r.h.s of Eq. (5) vanishes due to the Gauss's law, and so $\omega_n$ are found from $\lambda_n(\omega_n)=-1$.

In the presence of Ohmic losses, the mode eigenfrequencies acquire imaginary correction, $\omega_n'=\omega_n-i\gamma_n/2$, which can be found by including the imaginary part of polarization operator, $\hat{P}''$, in Eq. (4). For $q_n=\omega_n/\gamma_n\gg1$, the correction $\delta\lambda_n$ to the eigenvalue is small and, in the first order in $1/q_n$, the eigenfunctions are unchanged. The new eigenfrequency condition reads $1+\lambda_n+\delta\lambda_n=0$, where $\delta\lambda_n=i\lambda_n\langle n|\hat{P}''|n\rangle/\langle n|\hat{P}'|n\rangle$. Using the expansion $\lambda_n(\omega_n')=\lambda_n(\omega_n)-i(\gamma_n/2)\left[\partial\lambda_n(\omega_n)/\partial\omega_n\right]$ together with $\lambda_n(\omega_n)=-1$, we finally obtain the mode decay rate as

$$\gamma_n=-2\left(\frac{\partial\lambda_n}{\partial\omega_n}\right)^{-1}\frac{\langle n|\hat{P}''|n\rangle}{\langle n|\hat{P}'|n\rangle}=\frac{Q_n}{U_n},\quad(6)$$

where we introduced the mode energy

$$U_n=\frac{\omega_n}{2}\frac{\partial\lambda_n}{\partial\omega_n}\langle n|\hat{P}'|n\rangle=-\frac{\omega_n}{2}\frac{\partial\lambda_n}{\partial\omega_n}\mathrm{Re}\int dV\mathbf{E}_n\cdot\mathbf{P}_n,\quad(7)$$

and the absorbed power

$$Q_n=-\omega_n\langle n|\hat{P}''|n\rangle=\omega_n\mathrm{Im}\int dV\mathbf{E}_n\cdot\mathbf{P}_n.\quad(8)$$

Note that although the eigenstates and eigenvalues in Eq. (4) are defined for a local form of $\hat{P}'$, the corrections $\delta\lambda_n$, originating from $\hat{P}''$, may include nonlocal effects as well. In Eq. (7), the $\omega$ dependence of $\lambda_n$ comes from the *metallic* regions, i.e., $\partial\lambda_n/\partial\omega_n=\sum_m(\partial\lambda_n/\partial\varepsilon_m')(\partial\varepsilon_m'/\partial\omega_n)$, and using $\mathbf{P}_n=\mathbf{E}_n[\varepsilon(\omega_n,\boldsymbol{r})-1]/4\pi$, where the first term vanishes to due to the Gauss's law, we write

$$U_n=\frac{\omega_n}{8\pi}\sum_m\frac{\partial\varepsilon_m'}{\partial\omega_n}\frac{\partial\lambda_n}{\partial\varepsilon_m'}\int dV\mathbf{E}_n^2.\quad(9)$$

Then, using $(\partial\lambda_n/\partial\varepsilon_m')\int dV\mathbf{E}_n^2=\int dV_m\mathbf{E}_n^2$ [see Eq. (5)], we recover the usual expression for the mode energy [53],

$$U_n=\frac{\omega_n}{8\pi}\sum_m\frac{\partial\varepsilon_m'}{\partial\omega_n}\int dV_m\mathbf{E}_n^2=\int\frac{dV}{8\pi}\frac{\partial(\omega_n\varepsilon')}{\partial\omega_n}\mathbf{E}_n^2.\quad(10)$$

Similarly, the absorbed power (8) takes the form

$$Q_n=\frac{\omega_n}{4\pi}\int dV\varepsilon''(\omega_n,\boldsymbol{r})\mathbf{E}_n^2(\boldsymbol{r})+Q_n^{nl},\quad(11)$$

where $Q_n^{nl}$ includes non-local contributions, e.g., due to electron-hole pairs excitation near the metal-dielectric interface [54]. Here we consider the local case only and disregard $Q_n^{nl}$ in what follows. The integrals in Eqs. (10) and (11) are, in fact, carried over the metallic regions, and, for a single metallic region, we recover the plasmon bulk decay rate: $\gamma_n=2\varepsilon_m''(\omega_n)/[\partial\varepsilon_m'(\omega_n)/\partial\omega_n]$.

We now turn to the Green's function $\hat{G}$ for potentials, satisfying $(\Delta+4\pi\hat{P})G(\boldsymbol{r},\boldsymbol{r}')=-4\pi\delta(\boldsymbol{r}-\boldsymbol{r}')$, and split it

into Coulomb and plasmon terms as $\hat{G} = \hat{u} + \hat{G}_p$, where the latter is determined by $(\Delta + 4\pi\hat{P})\hat{G}_p = -4\pi\hat{P}\hat{u}$. Expanding $\hat{G}_p$ over the eigenstates of $\hat{P}'$ as $G_p(\omega;\boldsymbol{r},\boldsymbol{r}') = \sum_n G_n^p(\omega)\,\Phi_n(\boldsymbol{r})\Phi_n(\boldsymbol{r}')$, the coefficients are found as

$$G_n^p(\omega) = \frac{\lambda_n(\omega)}{\langle n|\hat{P}'|n\rangle}\frac{\lambda_n(\omega)+\delta\lambda_n(\omega)}{1+\lambda_n(\omega)+\delta\lambda_n(\omega)}, \qquad (12)$$

and exhibit plasmon resonances. Near a resonance at $\omega_n$, expanding $\lambda_n(\omega) = \lambda_n(\omega_n) + (\partial\lambda_n/\partial\omega_n)(\omega-\omega_n)$, using Eqs. (7)-(10), we obtain $G_n^p = g_n/(\omega-\omega_n+i\gamma_n/2)$, where $g_n = \omega_n/2U_n$ is the oscillator strength reflecting the fact that it is $U_n$, rather than $\hbar\omega_n$, that represent the mode energy in dispersive medium [53]. Similarly, the Green dyadic $\bar{\mathbf{D}}(\omega;\boldsymbol{r},\boldsymbol{r}') = \boldsymbol{\nabla}\otimes\boldsymbol{\nabla}'G(\omega;\boldsymbol{r},\boldsymbol{r}')$, which matches the near-field limit of $(-4\pi\omega^2/c^2)\bar{\mathbf{G}}(\omega;\boldsymbol{r},\boldsymbol{r}')$, is also a sum of Coulomb and plasmon terms, $\bar{\mathbf{D}} = \bar{\mathbf{D}}_0 + \bar{\mathbf{D}}_p$. For well resolved modes, the plasmon Green dyadic $\bar{\mathbf{D}}_p$ is dominated by the *resonant* mode, and we finally obtain

$$\bar{\mathbf{D}}_p(\omega;\boldsymbol{r},\boldsymbol{r}') = \frac{\omega_n}{2U_n}\frac{\mathbf{E}_n(\boldsymbol{r})\otimes\mathbf{E}_n(\boldsymbol{r}')}{\omega-\omega_n+i\gamma_n/2}. \qquad (13)$$

Note that the plasmon Green dyadic satisfies the optical theorem, $\int dV_1\varepsilon''(\omega,\boldsymbol{r}_1)\bar{\mathbf{D}}_p^*(\omega;\boldsymbol{r},\boldsymbol{r}_1)\cdot\bar{\mathbf{D}}_p(\omega;\boldsymbol{r}_1,\boldsymbol{r}') = -4\pi\bar{\mathbf{D}}_p''(\omega;\boldsymbol{r},\boldsymbol{r}')$, indicating the consistency of Eq. (13).

Correspondingly, the plasmon LDOS, defined as $\rho(\omega,\boldsymbol{r}) = -(1/2\pi^2\omega)\mathrm{Tr}\,\bar{\mathbf{D}}_p''(\omega;\boldsymbol{r},\boldsymbol{r})$ to match the near-field electromagnetic LDOS, has the Lorentzian shape

$$\rho(\omega,\boldsymbol{r}) = \frac{\gamma_n}{8\pi^2U_n}\frac{\mathbf{E}_n^2(\boldsymbol{r})}{(\omega-\omega_n)^2+\gamma_n^2/4}. \qquad (14)$$

Frequency integration of Eq. (14) yields, with help of Eq. (10), the plasmon mode density,

$$\rho(\boldsymbol{r}) = \int d\omega\rho(\omega,\boldsymbol{r}) = \frac{2\mathbf{E}_n^2(\boldsymbol{r})}{\int dV[\partial(\omega_n\varepsilon')/\partial\omega_n]\mathbf{E}_n^2}, \qquad (15)$$

which describes spatial distribution of plasmon states and, for typical $\mathbf{E}_n(\boldsymbol{r})$, represents the inverse plasmon mode volume [25, 55]. Near the resonance ($|\omega-\omega_n| \ll \gamma_n$), the plasmon LDOS takes the form

$$\rho(\omega_n,\boldsymbol{r}) = \frac{\mathbf{E}_n^2(\boldsymbol{r})}{2\pi^2U_n\gamma_n} = \frac{\mathbf{E}_n^2(\boldsymbol{r})}{2\pi^2Q_n}, \qquad (16)$$

where $Q_n$ is given by Eq. (11) and we used $\gamma_n = Q_n/U_n$ [see Eq. (6)]. Remarkably, the mode energy $U_n$ cancels out, and $\rho(\omega_n,\boldsymbol{r})$ is proportional to the local field intensity normalized by the absorbed power. In a similar manner, for CDOS near the plasmon resonance we obtain $\rho(\omega_n,\boldsymbol{r},\boldsymbol{r}') = (2\pi^2Q_n)^{-1}\mathbf{E}_n(\boldsymbol{r})\mathbf{E}_n(\boldsymbol{r}')$. Note that we used the real eigenmodes of Eq. (4); for local fields in complex form, Eqs. (10), (11), (13) and (16) (and the above CDOS) are multiplied by 1/2, but in either case, the plasmon LDOS has the universal form (1).

***Applications to energy transfer.***—Below, we apply our results to ET between QEs and plasmons as well as between donors and acceptors near a plasmonic structure. Consider a QE with the dipole moment $\mathbf{p} = \mu\boldsymbol{n}$ ($\mu$ is the dipole matrix element and $\boldsymbol{n}$ is its orientation) interacting with a resonant plasmon mode [see Fig. 1(a)]. The QE-plasmon ET rate $\Gamma = (2/\hbar)\mathrm{Im}[\boldsymbol{p}^*\cdot\mathbf{E}(\boldsymbol{r})]$, where $\mathbf{E}(\boldsymbol{r}) = -\bar{\mathbf{D}}(\omega_n;\boldsymbol{r},\boldsymbol{r})\cdot\boldsymbol{p}$ is the QE local field, has the standard form $\Gamma = (4\pi^2\mu^2\omega_n/3\hbar)\,\bar{\rho}(\omega_n,\boldsymbol{r})$ [15], where

$$\bar{\rho}(\omega_n,\boldsymbol{r}) = \frac{-3}{2\pi^2\omega_n}\,\boldsymbol{n}\cdot\bar{\mathbf{D}}''(\omega_n;\boldsymbol{r},\boldsymbol{r})\cdot\boldsymbol{n} = \frac{6}{\pi\omega_n}\frac{|\boldsymbol{n}\cdot\mathbf{E}_n(\boldsymbol{r})|^2}{\int dV\varepsilon''|\mathbf{E}_n|^2}, \qquad (17)$$

is the *projected* plasmon LDOS (hereafter, we adopt complex field notations), yielding

$$\Gamma = \frac{8\pi\mu^2}{\hbar}\frac{|\mathbf{n}\cdot\mathbf{E}_n(\boldsymbol{r})|^2}{\int dV\varepsilon''|\mathbf{E}_n|^2}. \qquad (18)$$

The rate increases when the losses are reduced, i.e., the plasmon resonance becomes sharper.

To verify Eq. (18), let us recover the QE-plasmon ET rate for a spherical metal NP [56]. The eigenmodes inside and outside the NP have the form $\mathbf{E}_{lm}(\boldsymbol{r}) \propto \boldsymbol{\nabla}[r^lY_{lm}(\hat{\boldsymbol{r}})]$ and $\mathbf{E}_{lm}(\boldsymbol{r}) \propto a^{2l+1}\boldsymbol{\nabla}[r^{-l-1}Y_{lm}(\hat{\boldsymbol{r}})]$, respectively, where $a$ is NP radius, $Y_{lm}(\hat{\boldsymbol{r}})$ are the spherical harmonics ($l$ and $m$ are polar and azimuthal numbers), and the eigenfrequencies $\omega_l$ satisfy $l\varepsilon_m'(\omega_l)+l+1=0$. For a QE oriented, e.g., normally to NP surface, we obtain

$$\Gamma_l = (2l+1)\frac{(l+1)^2}{l\varepsilon_m''(\omega_l)}\frac{2\mu^2}{\hbar}\frac{a^{2l+1}}{r^{2l+4}}. \qquad (19)$$

In Fig. 1(a), we plot the distance dependence of LDOS for a spheroidal NP normalized by spherical NP LDOS.

Consider now an *ensemble* of QEs near a plasmonic nanostructure. The plasmon-induced spatial correlations between QEs lead to cooperative effects [57, 58], and the ET rates are given by the eigenvalues of the decay matrix $\Gamma_{ij} = (4\pi^2\mu^2\omega_n/3\hbar)\bar{\rho}(\omega_n;\boldsymbol{r}_i,\boldsymbol{r}_j)$, where $\bar{\rho}(\omega;\boldsymbol{r}_i,\boldsymbol{r}_j) = -(3/2\pi^2\omega)\,\boldsymbol{n}_i\cdot\bar{\mathbf{D}}''(\omega;\boldsymbol{r}_i,\boldsymbol{r}_j)\cdot\boldsymbol{n}_j$ is the projected CDOS ($\boldsymbol{r}_i$ and $\boldsymbol{n}_i$ are, respectively, the QEs' positions and orientations). Using the single-mode chain rule for CDOS, $\bar{\rho}_n(\omega_n;\boldsymbol{r}_i,\boldsymbol{r}_j)\bar{\rho}_n(\omega_n;\boldsymbol{r}_j,\boldsymbol{r}_k) = \bar{\rho}_n(\omega_n;\boldsymbol{r}_i,\boldsymbol{r}_k)\bar{\rho}_n(\omega_n,\boldsymbol{r}_j)$, the cooperative ET rate can be found as

$$\Gamma^c = \frac{4\pi^2\mu^2\omega_n}{3\hbar}\sum_i\bar{\rho}(\omega_n,\boldsymbol{r}_i) = \sum_i\Gamma_i, \qquad (20)$$

with individual rates given by Eq. (18). As expected, $\Gamma^c$ scales linearly with the ensemble size.

We now turn to ET between a *donor* and an *acceptor* located at $\boldsymbol{r}_d$ and $\boldsymbol{r}_a$, respectively, near a plasmonic structure [see Fig. 1(b)]. The rate of direct (Förster) ET due to donor-acceptor dipole coupling, $\Gamma_{ad}^F$, normalized to the donor radiative decay rate $\gamma_r$, has the form [15]

$$\frac{\Gamma_{ad}^F}{\gamma_r} = \frac{9c^4}{8\pi}\int\frac{d\omega}{\omega^4}f_d(\omega)\sigma_a(\omega)|T_{ad}^0|^2 = \left(\frac{r_F}{r_{ad}}\right)^6, \qquad (21)$$

where $f_d(\omega)$ and $\sigma_a(\omega)$ are, respectively, the donor spectral function and the acceptor absorption crossection, $T^0_{ad} = -\boldsymbol{n}_a \cdot \bar{\mathbf{D}}_0(\boldsymbol{r}_a - \boldsymbol{r}_d) \cdot \boldsymbol{n}_d = s_{ad}/r^3_{ad}$ is the transition matrix element [$\boldsymbol{r}_{ad} = \boldsymbol{r}_a - \boldsymbol{r}_d$ is donor-acceptor distance and $s_{ad}$ is the orientational factor], and $r^6_F = (9c^4 s^2_{ad}/8\pi)\int d\omega f_d(\omega)\sigma_a(\omega)/\omega^4$ defines the Förster distance $r_F$ via the QEs' spectral overlap. The plasmon ET channel is included into Eq. (21) by replacing $T^0_{ad}$ with $T_{ad} = T^0_{ad} + T^p_{ad}$, where $T^p_{ad} = -\boldsymbol{n}_a \cdot \bar{\mathbf{D}}_p(\omega; \boldsymbol{r}_a, \boldsymbol{r}_d) \cdot \boldsymbol{n}_d$ is plasmon contribution to the matrix element [35–38]. Typically, the QEs' bands overlap well within a much broader plasmon band [6–8], so that $\bar{\mathbf{D}}_p$ can be taken at the resonance $\omega_n$. Then, the matrix element is related to the projected CDOS as $T^p_{ad} = (2i/3)\pi^2\omega_n\bar{\rho}(\omega_n; \boldsymbol{r}_a, \boldsymbol{r}_d)$, and, using the above chain rule, we obtain the donor-acceptor ET rate as $\Gamma_{ad} = \Gamma^F_{ad} + \Gamma^p_{ad}$, where

$$\frac{\Gamma^p_{ad}}{\gamma_r} = \frac{4\pi^4 r^6_F}{9 s^2_{ad}}\,\omega^2_n\,\bar{\rho}(\omega_n, \boldsymbol{r}_a)\bar{\rho}(\omega_n, \boldsymbol{r}_d) \tag{22}$$

is the plasmon-assisted ET rate. Importantly, $\Gamma^p_{ad}$ is proportional to the LDOS *product* at the donor and acceptor positions and, therefore, exhibits a donor-acceptor symmetry. To gain more insight, let us express $\Gamma^p_{ad}$ in terms of individual QE-plasmon ET rates (18) as

$$\frac{\Gamma^p_{ad}}{\gamma_r} = \left(\frac{\hbar\Gamma_a}{2U_F}\right)\left(\frac{\hbar\Gamma_d}{2U_F}\right), \tag{23}$$

where $U_F = \mu^2 s_{ad}/r^3_F$ is the dipole interaction at the Förster distance. Factorization of the donor-acceptor ET rate into rates of the constituent processes reflects the incoherent nature of ET between different QEs.

While Förster ET is efficient for small donor-acceptor distances, the system transitions to plasmon-dominated ET regime as $r_{ad}$ increases [6–8]. The transition onset is reached when $\Gamma^p_{ad} \gtrsim \Gamma^F_{ad}$, or, using Eqs. (21) and (23),

$$\left(\frac{\hbar\Gamma_a}{2U_{ad}}\right)\left(\frac{\hbar\Gamma_d}{2U_{ad}}\right) \gtrsim 1, \tag{24}$$

where $U_{ad} = \mu^2 s_{ad}/r^3_{ad}$ is the donor-acceptor dipole interaction, i.e., the *widths* associated with individual ET processes exceed the direct QE coupling. The explicit LDOS dependence of the ET rate allows us to derive, in general form, the plasmon enhancement factor for Förster ET, $\Gamma_{ad}/\Gamma^F_{ad}$. After averaging Eq. (22), i.e., replacing $\bar{\rho}$ with $\rho$ and $s^2_{ad}$ with 2/3, and using Eq. (1), we obtain

$$\frac{\Gamma_{ad}}{\Gamma^F_{ad}} = 1 + \frac{3}{2}\left[\frac{V_{ad}\,|\mathbf{E}_n(\boldsymbol{r}_a)|^2}{\int dV\varepsilon''|\mathbf{E}_n|^2}\right]\left[\frac{V_{ad}\,|\mathbf{E}_n(\boldsymbol{r}_d)|^2}{\int dV\varepsilon''|\mathbf{E}_n|^2}\right], \tag{25}$$

where $V_{ad} = 4\pi r^3_{ad}/3$ is spherical volume associated with $r_{ad}$. The ET enhancement factor depends solely on the local field distribution in the system, and, therefore, can be varied in a wide range with changing the system shape.

In Fig. 1(b), we plot $\Gamma_{ad}/\Gamma^F_{ad}$ for a donor and an acceptor at a distance $d$ from the opposite poles of a spheroidal NP. As the NP shape changes from a sphere to a thin nanorod, the ET rate increases by several orders of magnitude reflecting the change in LDOS that governs the individual QE-plasmon ET rates [see Fig. 1(a)].

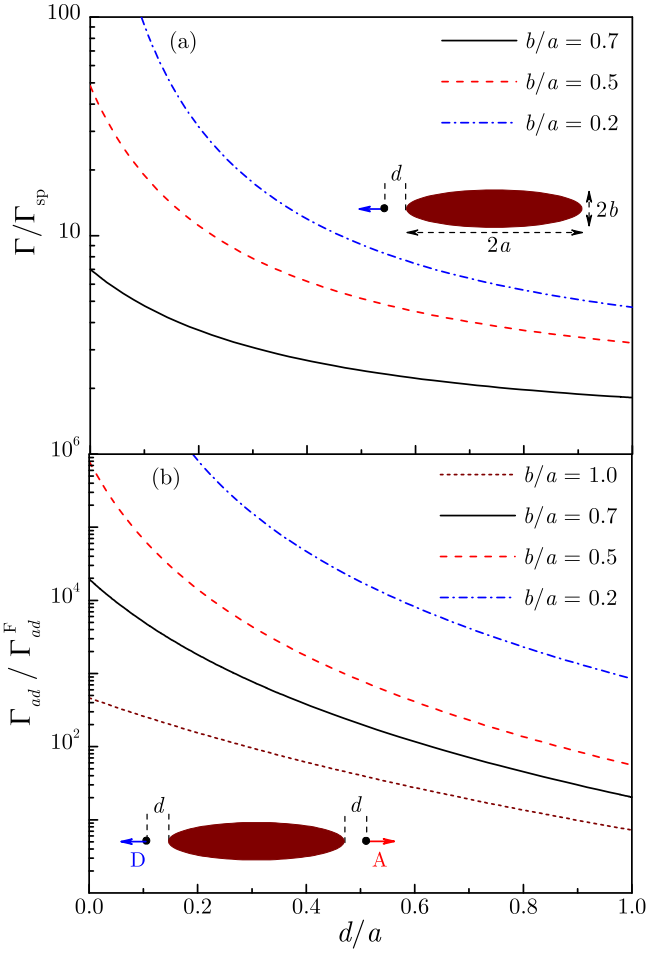


FIG. 1. (Color online) (a) Normalized QE-plasmon ET rate and (b) plasmon enhancement of Förster ET rate for QEs near the poles of a spheroidal NP with aspect ratio $b/a$.

If ET takes place between the ensembles of donors and acceptors near a plasmonic structure, the plasmon contribution to the ET rate factorizes into a product of rates for two constituent cooperative processes: an ET from donors to a resonant plasmon mode followed by ET from the plasmon mode to acceptors. The ET rate between two ensembles is given by Eq. (23), where individual rates $\Gamma_a$ and $\Gamma_d$ are replaced with their cooperative counterparts $\Gamma^c_a$ and $\Gamma^c_d$, given by Eq. (20).

In summary, the LDOS for any nanoplasmonic system has the universal form (1) in the frequency region dominated by plasmon resonance. Explicit formulae, in terms of the plasmon local field, are derived for ET between QEs and plasmons as well as between donors and acceptors situated near a plasmonic nanonostructure.

This work was supported in part by NSF grants No. DMR-1610427 and No. HRD-1547754.

[1] M. I. Stockman, *Nanoplasmonics: From Present into Future*, in *Plasmonics: Theory and Applications*, edited by T. V. Shahbazyan and M. I. Stockman (Springer, New York, 2013).

[2] E. C. Le Ru and P. G. Etchegoin, *Principles of Surface-Enhanced Raman Spectroscopy* (Elsevier, 2009).

[3] E. Dulkeith, A. C. Morteani, T. Niedereichholz, T. A. Klar, J. Feldmann, S. A. Levi, F. C. J. M.. van Veggel, D. N. Reinhoudt, M. Moller, and D. I. Gittins, Phys. Rev. Lett. **89**, 203002 (2002).

[4] P. Anger, P. Bharadwaj, and L. Novotny, Phys. Rev. Lett. **96**, 113002 (2006).

[5] S. Kühn, U. Hakanson, L. Rogobete, and V. Sandoghdar, Phys. Rev. Lett. **97**, 017402 (2006).

[6] J. R. Lakowicz, J. Kusba, Y. Shen, J. Malicka, S. DAuria, Z. Gryczynski, I. Gryczynski, J. Fluoresc. **13**, 69 (2003).

[7] P. Andrew and W. L. Barnes, Science **306**, 1002 (2004).

[8] M. Lunz, V. A. Gerard, Y. K. Gunko, V. Lesnyak, N. Gaponik, A. S. Susha, A. L. Rogach, and A. L. Bradley, Nano Lett. **11**, 3341 (2011).

[9] J. Bellessa, C. Bonnand, J. C. Plenet, and J. Mugnier, Phys. Rev. Lett. **93**, 036404 (2004).

[10] Y. Sugawara, T. A. Kelf, J. J. Baumberg, M. E. Abdelsalam, and P. N. Bartlett, Phys. Rev. Lett. **97**, 266808 (2006).

[11] N. T. Fofang, T.-H. Park, O. Neumann, N. A. Mirin, P. Nordlander, and N. J. Halas, Nano Lett. **8**, 3481 (2008).

[12] D. J. Bergman and M. I. Stockman, Phys. Rev. Lett., **90**, 027402, (2003).

[13] M. A. Noginov, G. Zhu, A. M. Belgrave, R. Bakker, V. M. Shalaev, E. E. Narimanov, S. Stout, E. Herz, T. Suteewong and U. Wiesner, Nature, **460**, 1110, (2009).

[14] R. F. Oulton, V. J. Sorger, T. Zentgraf, R.-M. Ma, C. Gladden, L. Dai, G. Bartal, and X. Zhang, Nature **461**, 629, (2009).

[15] L. Novotny and B. Hecht, *Principles of Nano-Optics* (CUP, New York, 2012).

[16] E. M. Purcell, Phys. Rev. **69** (1946) 681.

[17] A. Dereux, C. Girard, and J. C. Weeber, J. Chem. Phys. **112**, 7775 (2000).

[18] K. Joulain, R. Carminati, J.-P. Mulet, and J.-J. Greffet, Phys. Rev. B **68**, 245405 (2003).

[19] M. Kuttge, E. J. R. Vesseur, A. F. Koenderink, H. J. Lezec, H. A. Atwater, F. J. Garcia de Abajo, and A. Polman, Phys. Rev. B **79**, 113405 (2009).

[20] V. Krachmalnicoff, E. Castanié, Y. De Wilde, and R. Carminati, Phys. Rev. Lett. **105**, 183901 (2010).

[21] M. A. Noginov, H. Li, Yu. A. Barnakov, D. Dryden, G. Nataraj, G. Zhu, C. E. Bonner, M. Mayy, Z. Jacob, and E. E. Narimanov, Opt. Lett. **35**, 1863 (2010).

[22] A. N. Poddubny, P. A. Belov, P. Ginzburg, A. V. Zayats, and Y. S. Kivshar, Phys. Rev. B **86**, 035148 (2012).

[23] R. Carminati, J. J. Greffet, C. Henkel, J. M. Vigoureux, Opt. Commun. **261** 368 (2006).

[24] N. Lawrence and L. Dal Negro, Opt. Express **18**, 16120 (2010).

[25] C. Sauvan, J. P. Hugonin, I. S. Maksymov, and P. Lalanne, Phys. Rev. Lett. **110**, 237401 (2013).

[26] R. Carminati, A. Cazé, D. Cao, F. Peragut, V. Krachmalnicoff, R. Pierrat, Y. De Wilde, Surf. Sci. Rep. **70**, 41 (2015).

[27] A. Cazé, R. Pierrat, and R. Carminati, Phys. Rev. Lett. **110**, 063903 (2013).

[28] H. M. Lai, P. T. Leung, K. Young, P. W. Barber, and S. C. Hill, Phys. Rev. A **41**, 5187 (1990).

[29] P. T. Kristensen, C. Van Vlack, and S. Hughes, Opt. Lett. **37**, 1649 (2012).

[30] C. Sauvan, J. P. Hugonin, R. Carminati, and P. Lalanne, Phys. Rev. A **89**, 043825 (2014).

[31] P. T. Kristensen, R.-C. Ge, and S. Hughes, Phys. Rev. A **92**, 053810 (2015).

[32] J. R. Lakowicz, Anal. Biochem. **298**, 1 (2001).

[33] J. Zhao, X. Zhang, C. Yonzon, A. J. Haes, and R. P. Van Duyne, Nanomedicine **1**, 219 (2006).

[34] T. Förster, Ann. Phys. **437**, 55 (1948).

[35] J. I. Gersten and A. Nitzan, Chem. Phys. Lett. **104**, 31 (1984).

[36] H. T. Dung, L. Knöll, and D.-G. Welsch, Phys. Rev. A **65**, 043813 (2002).

[37] G. Colas des Francs, C. Girard, and O. J. F. Martin, Phys. Rev. A **67**, 053805 (2003).

[38] V. N. Pustovit, T. V. Shahbazyan, Phys. Rev. B **83**, 085427 (2011).

[39] M. J. A. de Dood, J. Knoester, A. Tip, A. Polman, Phys. Rev. B **71**, 115102 (2005).

[40] T. Nakamura, M. Fujii, S. Miura, M. Inui, and S. Hayashi, Phys. Rev. B **74**, 045302 (2006).

[41] R. Vincent and R. Carminati, Phys. Rev. B **83**, 165426 (2011).

[42] J. Enderlein, Int. J. Mol. Sci. **13**, 15227 (2012).

[43] C. Blum, N. Zijlstra, A. Lagendijk, M. Wubs, A. P. Mosk, V. Subramaniam, W. L. Vos, Phys. Rev. Lett. **109**, 203601 (2012).

[44] F. T. Rabouw, S. A. den Hartog, T. Senden, A. Meijerink, Nature Commun. **5**, 3610 (2014).

[45] P. Ghenuche, J. de Torres, S. B. Moparthi, V. Grigoriev, J. Wenger, Nano Lett. **14**, 4707 (2014).

[46] T. U. Tumkur, J. K. Kitur, C. E. Bonner, A. N. Poddubny, E. E. Narimanov, M. A. Noginov, Faraday Discussions **178**, 395 (2014).

[47] M. Wubs, W. L. Vos, New J. Phys. **18**, 053037 (2016).

[48] A. Manjavacas, F. J. Garcia de Abajo, and P. Nordlander, Nano Lett. **11**, 2318 (2011).

[49] A. Delga, J. Feist, J. Bravo-Abad, and F. J. Garcia-Vidal, Phys. Rev. Lett. **112**, 253601 (2014).

[50] M. I. Stockman, J. Opt. **12**, 024004, (2010).

[51] See, e.g., G. D. Mahan, *Many-Particle Physics* (Plenum, New York, 1990).

[52] G. Boudarham and M. Kociak, Phys. Rev. B **85**, 245447 (2012).

[53] L. D. Landau and E. M. Lifshitz, *Electrodynamics of Continuous Media* (Elsevier, Amsterdam, 2004).

[54] A. S. Kirakosyan, M. I. Stockman, and T. V. Shahbazyan, arXiv:0908.0647.

[55] S. Maier, Opt. Express 14, 1957 (2006).

[56] R. Ruppin, J. Chem. Phys. **76**, 1681 (1982).

[57] V. N. Pustovit, T. V. Shahbazyan, Phys. Rev. Lett. 102, 077401 (2009).

[58] V. N. Pustovit, T. V. Shahbazyan, Phys. Rev. B **82**, 075429 (2010).

[59] V. N. Pustovit, A. M. Urbas, T. V. Shahbazyan, Phys. Rev. B **88**, 245427 (2013).

[60] A. N. Poddubny Phys. Rev. B **92**, 155418 (2015).